(Received 10 March 2026, Accepted 22 April 2026, Scheduled 12 May 2026)

Design of Symmetric Quad Circular Radiator Antenna with Semi Circular Bridge and DGS for WLAN, ISM Band and Sub-6 GHz Applications

Prasanth K. Jujjarapu[1], Nallamothu Suneetha[2], Padavala A. Kumar[3], Akondi N. Kiran[4], and Bokkisam V. S. Sailaja[5,*]

[1]*Department of Electronics and Communication Engineering, Ramachandra College of Engineering, Eluru, Andhra Pradesh 534007, India*
[2]*Department of Electronics and Communication Engineering, Sir CR Reddy College of Engineering, Eluru, Andhra Pradesh 534007, India*
[3]*Department of Electronics and Communication Engineering, ICFAI Tech (Faculty of Science and Technology), ICFAI Foundation for Higher Education, Dontanapally, Hydrabad 501203, India*
[4]*Department of Electronics and Communication Engineering, New Horizon College of Engineering, Bengaluru, Karnataka, India*
[5]*Department of Electronics and Communication Engineering, KLEF (deemed to be University), Vaddeswaram, Guntur 522502, India*

ABSTRACT: The proposed symmetric quad circular radiator antenna with a semicircular etched-slot DGS was designed and fabricated on an FR4 substrate of size $50 \times 50 \times 1.6\,\text{mm}^3$. The antenna provides impedance bandwidths of 2.24–2.94 GHz, 3.84–3.98 GHz, and 4.92–5.06 GHz, with resonant frequencies observed at 2.44 GHz (−40.3 dB), 2.86 GHz (−17.9 dB), 3.92 GHz (−14.9 dB), and 4.98 GHz (−10.6 dB). These operating bands make the antenna suitable for WLAN, ISM, and other sub-6 GHz wireless communication systems. The antenna also achieves a realized gain above 5 dB at the operating frequencies, indicating stable radiation characteristics. The diversity performance was evaluated using standard metrics. The ECC remains below 0.5, which lies within the acceptable range for diversity operation. In addition, the diversity gain varies between 9.88 and 10.02 dB, while the channel capacity loss stays below 0.6 bits/s/Hz across the frequency range. A compact symmetric quad circular radiator antenna incorporating a three-segment semicircular bridge along with a semicircular etched-slot mdefected ground structure (DGS) is presented for multi-band wireless communication applications. These results confirm that the proposed antenna provides reliable radiation and diversity performance for practical wireless communication applications.

1. INTRODUCTION

Four-port MIMO circular patch antennas are widely used in modern wireless communication systems because they improve channel capacity, diversity performance, and link reliability. Channel capacity, diversity performance, and link reliability can be significantly improved using four-port multiple-input multiple-output (MIMO) circular patch antennas, making them an ideal solution for modern wireless communication systems. However, in the past few years, there has been significant interest in the design of wideband, compact MIMO antenna arrays that demonstrate robust isolation and stable radiation behavior for 5G, sub-6 GHz communication, ultra-wideband (UWB), and millimeter-wave systems.

Research was initially focused on improving isolation and safety in wearable and portable devices. In this field of research, a wearable UWB MIMO antenna with a parasitic element was proposed in [1]. Likewise, a small-sized, CPW-fed four-element UWB MIMO antenna was documented in [2], where the proper placement of the antenna elements was selected to minimize correlation between them while maintaining steady impedance matching across the whole UWB range. An optically transparent UWB antenna for automotive MIMO communication was presented in [3], demonstrating that transparency can be realized with little impact on radiation performance. In [4], a miniaturized quad-port MIMO antenna was fabricated around 11 GHz and 13 GHz with special focus on compactness and isolation improvements. In particular, a quad-port MIMO antenna was reported in [5], intended for sub-6 GHz 5G NR applications, with high isolation between closely spaced radiators. In [6], a MIMO antenna with circularly polarized radiation based on a hybrid technique was introduced and designed for Industrial, Scientific, and Medical (ISM) band (57–64 GHz) millimeter-wave systems. Besides, metasurface-based methods have been explored for mutual coupling reduction to enhance antenna performance [7], and a metasurface layer in combination with a four-port circularly polarized antenna array was presented in [8], achieving isolation and polarization control.

Advanced materials and electromagnetic structures have been investigated for enhancing antenna performance. A

* Corresponding author: Bokkisam Venkata Sai Sailaja (sailajabokkisam@gmail.com).

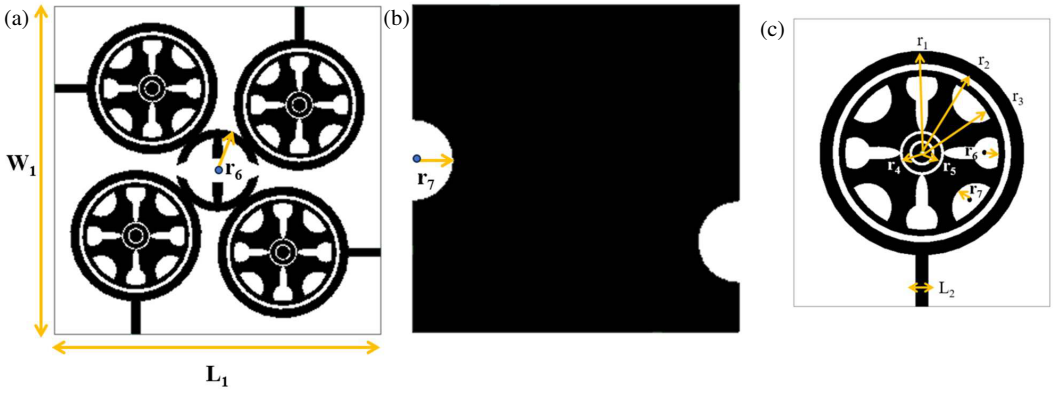

FIGURE 1. The SQCR-DGS design. (a) Top view. (b) Bottom view. (c) Single unit structure.

metamaterial lens antenna with a large aperture was reported as a multilayer MIMO transmission antenna [9, 10]. In [11], a small, dual-band four-port MIMO antenna covering many of the 5G and WLAN bands was proposed. Furthermore, deep learning-based surrogate modeling for phased array antennas was demonstrated in [12], which facilitated faster simulation and design of millimeter-wave antennas. Ref. [13] presented a compact dual-band MIMO antenna for smartphone applications in n79 and sub-7 GHz bands. Flexible on-package phased array antennas suited for massive MIMO communication in wearable 5G and millimeter-wave systems were reported in [14].

Advancements in transparent materials and novel decoupling architectures follow. Ref. [15] introduced a dual-band transparent antenna applicable to MIMO systems. In [16], a self-decoupling technique allowing antennas to be placed closely together without isolating structures has been presented. Also, self-decoupling ability was considered in work [17] for an eight-element shared-aperture MIMO antenna array, where SAR reduction and compact integration were also investigated.

Research has also been targeted toward compact, dual-band, and flexible antenna structures for modern wireless communication devices. In [18], a bendable inverted L-shaped antenna for sub-6 GHz 5G communication was introduced. The design of a four-directional Vivaldi-based MIMO antenna system for vehicle communication is described in [19]. Ref. [20] proposed another small-sized half-circular U-shaped MIMO antenna, providing good isolation and radiation efficiency. In [21], a compact 2×2 multiband MIMO antenna for sub-6 GHz communication is proposed, and in [22], a low-profile extended-wideband MIMO antenna based on CO-CSRR and EBG structures is introduced. An ultra-low-profile sub-6 GHz four-element MIMO antenna was presented in [23], which is optimized for impedance matching and isolation while maintaining a relatively compact size.

This paper includes the design of a compact quad-port MIMO antenna using a circular slot with wideband 5G applications. This design achieves reasonably good isolation and bandwidth for contemporary wireless systems [24].

This research is concerned with the isolation enhancement of MIMO antennas using a dedicated decoupling structure. Through the proposed technique, mutual coupling between elements can be minimized, leading to an increase in the overall antenna performance [25].

The proposed antenna consists of four symmetrically arranged circular radiators integrated with a semicircular etched-slot defected ground structure on an FR4 substrate. The parameters show ECC values below 0.5, diversity gain close to 10 dB, and channel capacity loss under 0.6 bits/s/Hz, indicating dependable operation for WLAN, ISM, and other sub-6 GHz wireless systems. The proposed antenna can realize multiband operation with a compact size and easy configuration. It is simpler than many existing designs, as it has no need for isolation elements or complex geometries. The central bridge and DGS provide better performance while maintaining a simple and efficient design for real-world applications. The lower band around 2.4 GHz corresponds to the WLAN and ISM band, which is widely used for applications such as Wi-Fi, Bluetooth, and IoT devices. The upper resonant bands in the sub-6 GHz range are used by new spectrum for modern wireless systems, including extended WLAN bands and new communication services at lower frequencies.

2. DESIGN DESCRIPTION

In the symmetric quad circular radiator defected ground structure (SQCR-DGS) antenna, shown in Fig. 1, a semicircular bridge is introduced at the centre of the four radiating elements, and a DGS is also designed in the ground plane to achieve the specified bands. The central part is electrically connected with the four patch elements and changes the current distribution in the nearby circular patches. Due to the central conductive bridge, the coupling between patches is increased. It also changes the effective electrical length, which is why it improves impedance matching, and extra modes are produced. The central etched-slot structure and DGS further reduce the unwanted currents generated. All of these features together lead the antenna to obtaining several frequency bands, which make the final configuration suitable for WLAN, ISM band, and sub-6 GHz applications.

This design originated as a set of four circles connected by radiator sections (Fig. 1), due to the current flow by circular shape and stable radiation. However, the structure provided limited bandwidth and fewer resonances. This was rectified by implementing internal slots within each radiator to establish further

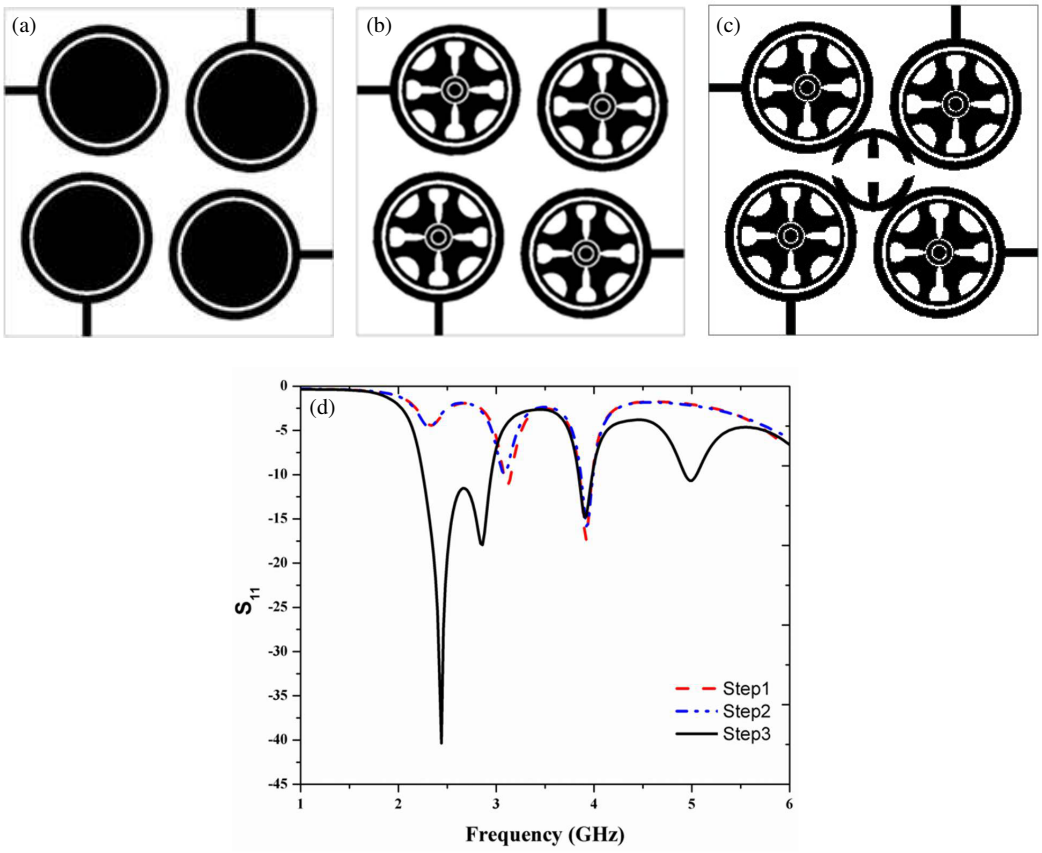

FIGURE 2. Evolution of the SQCR-DGS. (a) Step 1. (b) Step 2. (c) Step 3. (d) Simulated S_{11} (for all the steps).

current paths, allowing for multiband operation. The addition of the central semicircular bridge connected all four elements together and allowed current to flow between them, enhancing overall radiation behaviour without increasing the size. After the simulation of the current distribution, a series of semicircular cuts were introduced in the ground plane (DGS). It was noticed that there were concentrated areas with strong ground currents. Introducing these semicircular cuts altered the path of the ground return in a controlled manner, allowing for effective impedance matching and additional resonant frequency generation. The circular patches all meet in the middle and are connected by a semicircular bridge, giving a channel for current to flow between them. What previously would have caused each element to work independently, now spans throughout the structure, creating longer paths. This adds gently to coupling and allows the driving of further resonant modes on. The influence is seen in the present distribution, where we see these strong currents around the bridge region compared to earlier stages of design.

In Step-1 (Fig. 2(a)), four identical round patches ($r_1 = 10\,\text{mm}$) are symmetrically added to the surface. At this point, the electric current primarily travels along the edges of each circular spike. This value optimizes the current distribution between the inner and outer regions, resulting in improved impedance matching together with well-defined multiple resonances. In Step-2 (Fig. 2(b)) slots are placed at different distances inside each circular radiator (internal slots r_2, r_3, r_4, r_5 and r_7). These slots disrupt the continuous current path and require current to flow through many narrow channels. It increases the effective electrical length, resulting in multiple current loops inside each patch. This gives rise to other resonant frequencies observed. In Step-3 (Fig. 2(c)) a semicircular bridge ($r_6 = 7\,\text{mm}$) is connected at the centre between all four radiators and the ground plane has also the semicircular DGS ($r_7 = 1.9\,\text{mm}$). The bridge connects current among the four elements, rather than restricting this flow to individual patches. This causes heavy coupling and additional current paths that enhance impedance matchings and produce new resonating modes. Finally, the DGS modifies the ground current and suppresses undesirable surface waves, which could greatly enhance radiation and bandwidth stability.

In the first step, the structure has only a circular, symmetrical layout on the substrate. This simple step makes the antenna work similarly to a basic circular array, which can mainly provide a single resonance. The slots are developed inside each circular element. The established etched slots also modify the surface current distribution. Finally, the introduction of additional resonant bands leads to multiband behavior in the S_{11} response.

Step-3: A centre semicircular bridge is added between the circular elements with a DGS on the ground. After performing this update, the current flow is further affected, and more coupling paths are developed between the elements. Fig. 2(d) shows the comparison of all the steps in terms of S_{11}. The antenna sequence design for the two steps, based on improved antenna performance from Step-1 to Step-3, is satisfactorily de-

scribed in Fig. 2(d). The final design meets the target specifications for working at the WLAN, ISM band, and sub-6 GHz applications. The key parameters of the SQCR-DGS antenna are reported in Table 1.

TABLE 1. Key dimensions of SQCR-DGS geometry.

Dimension	Value (mm)	Dimension	Value (mm)
L_1	50	r_3	8
W_1	50	r_4	3.5
L_2	2	r_5	3
r_1	10	r_6	7
r_2	9	r_7	1.9

Inside each radiator, there are numerous internal slots (r_2–r_5), creating additional current paths and allowing the support for multiple resonant frequencies to be achieved within a single compact region. The central semicircular bridge (r_6) is another crucial element that unites all four radiators. This is in contrast to traditional MIMO antennas, where the elements are maintained separated. In this case, the bridge lets current smoothly flow between the elements and maintain multiband behaviour while keeping the dimensions small. Moreover, the semicircular DGS (r_7) in the ground plane is of particular design. It alters the ground current, which helps to achieve better impedance matching and provides additional resonances. Thus, the novelty comes from the joint effect of using slotted circular radiators (to create more resonance), a central bridge connection (to close resonator chains), and properly shaped DGS, all combined together in a compact structure of only $50 \times 50\,\text{mm}^2$ to reach multiband MIMO design.

3. RESULTS AND ANALYSIS

In this section, a comprehensive analysis of the S_{11} response in simulation and experimental results are presented. The reflection coefficient and transmission properties are studied to test the impedance matching as well as the multiband performance of the antenna. Co-pol and cross-pol performance for the simulated and measured radiation patterns is also presented. Additionally, diversity performance is measured in terms of the key MIMO parameters, including envelope correlation coefficient (ECC), diversity gain (DG), and channel characteristics calculated from S-parameters. We analyze the parameters S_{11}, S_{12}, S_{13}, and S_{14} to investigate the impedance matching and mutual coupling between circular elements. Further, a parametric study of various design parameters L_2, r_1, and r_4 is done with the aim of evaluating their impact on the performance of the antenna. The experimental structure is tested in an anechoic chamber to investigate its surface current distribution at all frequency bands. Near the two frequencies of 2.44 GHz and 2.86 GHz, most of the current is distributed along the edges of the circular patch elements and the feeding region. There are also strong current distributions at the central bridge, illustrating that this part contributes significantly to the lower resonance. Similarly, this area helps produce the second resonance without altering the radiation characteristics.

The current distribution changes at higher frequencies, 3.92 GHz and 4.998 GHz, contributing to the middle and higher operating bands, respectively. Such behaviours are shown and analysed in Fig. 3.

The fundamental current flow along the boundary of the outer circular radiator (r_1) mainly supports this resonance mode. The inner circular and slot features (r_2–r_5) disrupts this uniform path and direct the current through smaller loops inside the patch, generating further resonant modes at higher frequencies. The medium-sized semicircular bridge (r_6) connects all four radiators, which provide paths for the current continuum to travel from one element to another, effectively creating longer combined current paths that can help create new resonances. The reflection current is disturbed, and the distribution of this current changes in the ground plane as well when the semicircular DGS (r_7) causes better impedance matching and helps multi-band formations. So, all this defines the multiband behavior by the combination of outer edge currents atop and slot-induced inner loops; inter-element current sharing through the bridge between slots further helps achieve multiband property along with changing ground-formed current paths due to DGS.

The (Fig. 4(a)) parameter L_2, the length of the feed connection, is adjusted because it mainly influences how much power is effectively coupled from the feed line to a circular radiator. An increase in L_2 from 1.8 mm to 2.0 mm results in a relatively longer path from the feed to the patch. This enhances impedance matching, which can be seen as corresponding deeper S_{11} minima in the figure. A smoother transition between the feed and radiator enables more energy to be radiated and not internally reflected. The outer radius (Fig. 4(b)) r_1, which determines its dimension, of the circular radiator; since this parameter directly determines the effective electrical length of an antenna. The greater the radius is, the longer distance the surface current can flow along that circular boundary. This causes the resonant frequencies to move towards lower values. It is observed from Fig. 4(b) that when r_1 increases from 9.8 mm to 10 mm, the resonance becomes stronger due to improved current distribution over the circular patch. Parameter r_4 refers to the inner slot structure of a circular radiator. This parameter affects the distribution of current flowing within the patch instead of along the border. As r_4 increases, it creates additional current loops in the slot region, which alter the electromagnetic energy and radiation characteristics. This value optimizes the current distribution to balance between the inner and outer regions, achieving a poor impedance matching together with well-defined multiple resonances.

Figure 5 depicts the simulation response of design parameter r_4 on the SQCR-DGS reflection coefficient and its relevant S-parameters (from ports). To analyse the behaviour on the resonant characteristics, r_4 was changed in the range of 3.3 mm to 3.5 mm (Fig. 5(a)). The antenna shows stronger resonance within the lower band, and the case of $r_4 = 3.5$ mm allows for better impedance matching compared to other cases. Similarly, r_4 changes the effective current path of the circular radiator and slot region, hence affecting the resonance of the design.

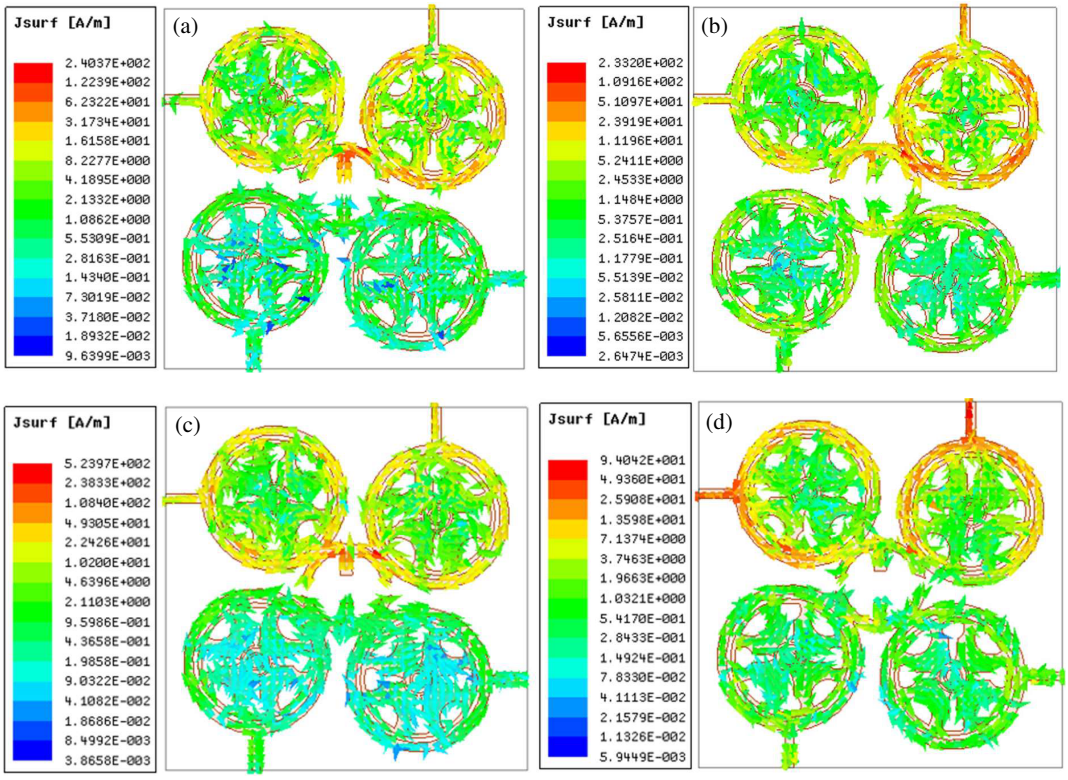

FIGURE 3. Simulated surface current distributions at two resonant frequencies. (a) 2.44 GHz, (b) 2.86 GHz, (c) 3.92 GHz, (d) 3.98 GHz.

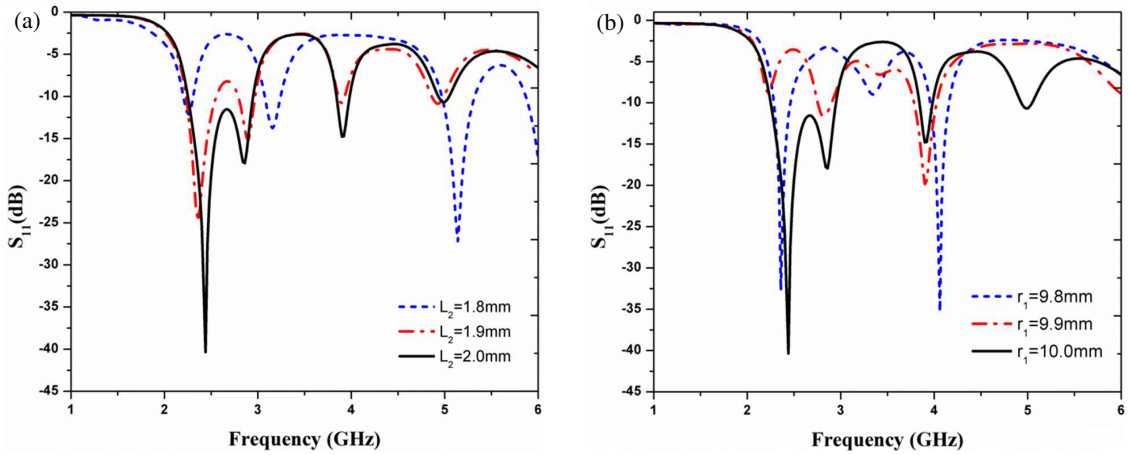

FIGURE 4. Simulated reflection coefficients of the proposed antenna with different parameter values. (a) L_2, (b) r_1.

Accordingly, the final configuration uses the optimal value of $r_4 = 3.5$ mm in order to achieve multiband behaviour.

In Fig. 5(b), it is observed that the coupling between ports 1 and 2 (S_{21}) is because these elements are close, with direct interaction through the semicircular bridge. The differences among S_{12}, S_{13}, and S_{14} result from the small asymmetry introduced by this bridge structure. As a result, the current distribution is uneven in the x and y directions, leading to different levels of coupling. However, this effect is to support multiband behaviour through additional current paths. Despite this asymmetry, the overall MIMO performance is acceptable owing to low ECC values. As can be seen in Fig. 5(b), the isolation between antenna elements for all operating bands is observed to be approximately -10 dB. Higher isolation is always preferred; however, the high isolation within a compact structure with tightly packed elements is hard to accomplish. This degree of isolation is suitable in the design model, since the antenna remains with quite low ECC (less than 0.1) as well as stable gain. This shows that overall MIMO performance is hardly dependent on mutual coupling. In Fig. 5(c), r_7 is varied in the antenna to see the impact of this parameter on S_{11}. The resonance points for the S_{11} mode shift slightly as r_7 varies from 1.7 mm to 1.9 mm, consistent with changes in their resonant frequencies. As can be observed with $r_7 = 1.9$ mm, it assists a deeper res-

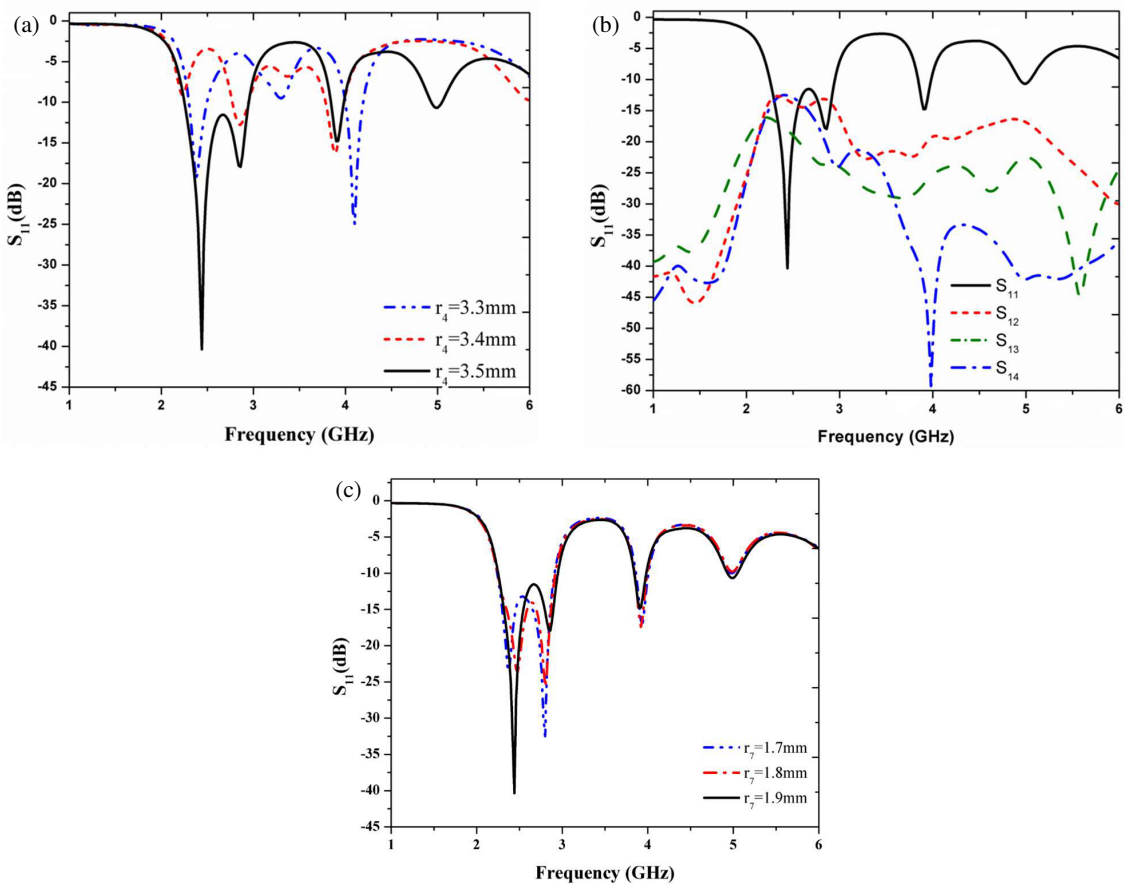

FIGURE 5. Simulated reflection coefficients of the proposed antenna with different values (a) r_4, (b) S-parameters response, (c) r_7.

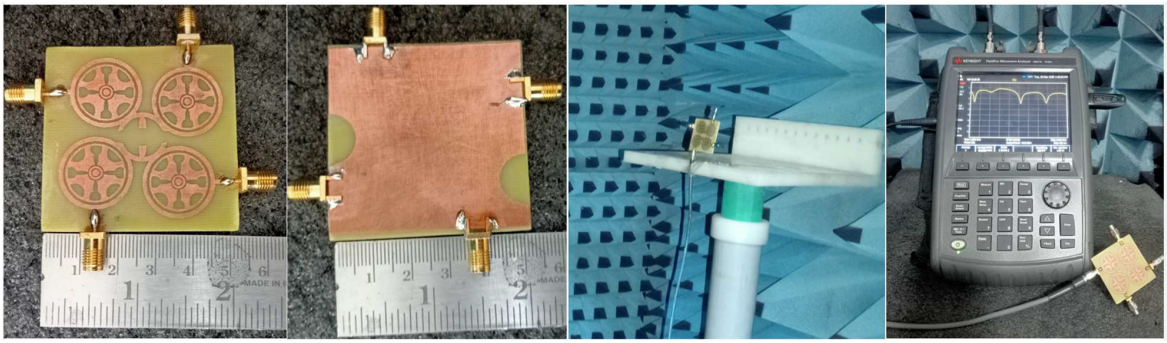

(a) (b)

FIGURE 6. Fabricated model of SQCR-DGS antenna. (a) Top view. (b) Bottom view with analyser.

onance at the lower band of the spectrum, which implies good impedance matching in that region, as also noted in the measurement results. This means that the DGS has significance in tuning the antenna performance and for multiband behavior.

The experimental setup of the prototyped antenna is presented in Fig. 6, with front and back views, and also includes an analyzer. The S_{11} (Sim. & Meas.) of the proposed SQCR-DGS antenna performance is presented in Fig. 7, which represents the reflection features between the different operating bands. The S_{21} (Sim. & Meas.) of the SQCR-DGS antenna as per the proposed design is shown in Fig. 8, representing the interaction and coupling arising from the ports during transmission. The measured results correlate well with the simulation with some variation mainly due to fabrication tolerances and measurement conditions.

The radiation patterns at various frequencies vary slightly in shape and direction due to the change in current distribution on the radiators. Four antenna elements are used, and we can expect slightly varying radiations from the antennas as they are arranged symmetrically but facing in four different directions. This brings pattern diversity, and it decreases the cross correlation of the antenna ports. Consequently, the antenna

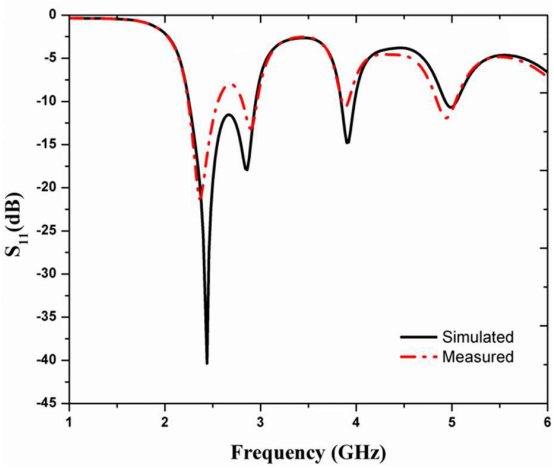

FIGURE 7. S_{11} (sim. & meas.) of the proposed SQCR-DGS antenna.

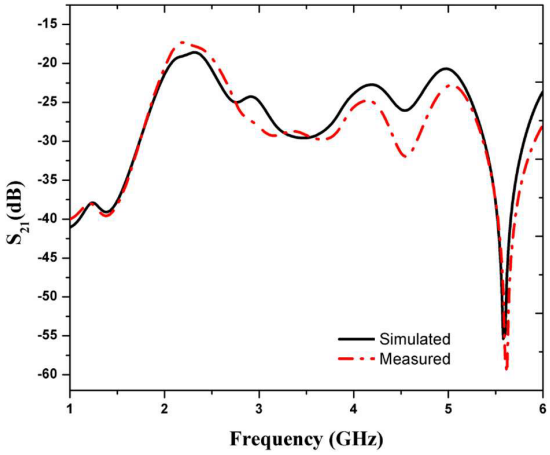

FIGURE 8. S_{21} (sim. & meas.) of the proposed SQCR-DGS antenna.

yields low ECC values and good diversity performance, making it suitable for MIMO applications. The radiating patterns of the proposed antenna at four operating frequencies, 2.44 GHz, 2.86 GHz, 3.92 GHz, and 4.98 GHz, are explained in Fig. 9.

Figure 10 shows the radiation of the SQCR-DGS antenna at all frequencies, including co-pol and cross-pol. The change in gain obtained from simulation and measurements against operating frequencies is shown in Fig. 10. The gain improves gradually with the increase in frequency. The simulated results show a gain starting slightly above 5 dBi at the lower end of the band and rising to nearly 6.3 dBi as it moves to higher frequencies. The measured curve shows a similar behaviour, despite slightly lower values than those of the simulated one. These differences, although small, are still noticeable over the two curves but remain fairly consistent because both curves show a predictable trend, thus indicating that the antenna radiates well across much of this working band.

Figure 11 shows the envelope correlation coefficient (ECC) calculated for the antenna. The ECC values are generally quite small and mainly in the range of less than 0.1 over the entire frequency span. Such low values suggest that there is very little interaction between the antenna elements, and they have almost independent radiation behaviour. There are also a few deep troughs at specific frequencies along the curve, implying better overall isolation between the elements around those points. While correlation is low in such systems, it is important for MIMO systems, as this helps preserve signal diversity and improves the reliability of the wireless communication link.

Under S-parameters, the ECC of the proposed antenna is evaluated as shown in Fig. 11. The ECC values are noted to be very low (often below 0.1) over the operating frequency bands. The low values suggest that the antenna elements function independently with minimal impact on each other. It ensures diversity performance and good signal transmission reliability in MIMO systems.

The ECC is computed from S-parameters, which gives a measure related to the correlation among the antenna elements.

The semicircular bridge provides asymmetry in the structure itself. This is done on purpose to generate extra current paths and provide multiband functionality. It influences the coupling levels, but still, the MIMO performance is acceptable. Simulations with and without the DGS were observed for comparison. If a complete ground plane is used, the antenna shows fewer resonant bands and weaker impedance matching. The semicircular DGS alters the ground current and enhances the multiband characteristics. Fabrication tolerance, connector losses, and measurement conditions cause small differences between simulated and measured results.

The diversity gain performance of the antenna system is shown in Fig. 12. The analysis clearly indicates that the DG value remains close to its optimal levels across the frequency, nearly 10 dB. Even though slight fluctuations do appear at some frequencies, the values stay limited within a very narrow band. This phenomenon explains that the antenna has suitable diversity potential that narrows the signal reduction associated with multipath. The multi-antenna wireless communication characteristic is verified by the relatively low and consistent DG response of about -0.25 dB across the frequency band from 20 to 68 GHz, which shows that it is well suited for use as a proposed antenna.

Figure 13 shows the radiation efficiencies of the simulated and measured antennas. Simulated efficiency shows similarly high values around 83–86% across the whole operational frequency band. The corresponding measured efficiency, while following a similar trend, is also lower from 78% to 82%. This discrepancy is expected in actual measurements and can result from conductor losses, dielectric losses of the substrate during fabrication. Regardless of these factors, the antenna demonstrates high efficiency, which means that most of the supplied power is converted into radiated electromagnetic energy. The MIMO parameter CCL is described in Fig. 14.

Table 2 explains the merits of our proposed antenna. The gain improvement is predominantly induced by symmetric geometry with four pointing circular radiators, to ensure that currents are flowing uniformly, and stability exists in radiation. The main half-circular bridge integrates all parts of the design and utilizes this to strengthen radiation without having a larger size. The compact structure is enabled by circular patches with

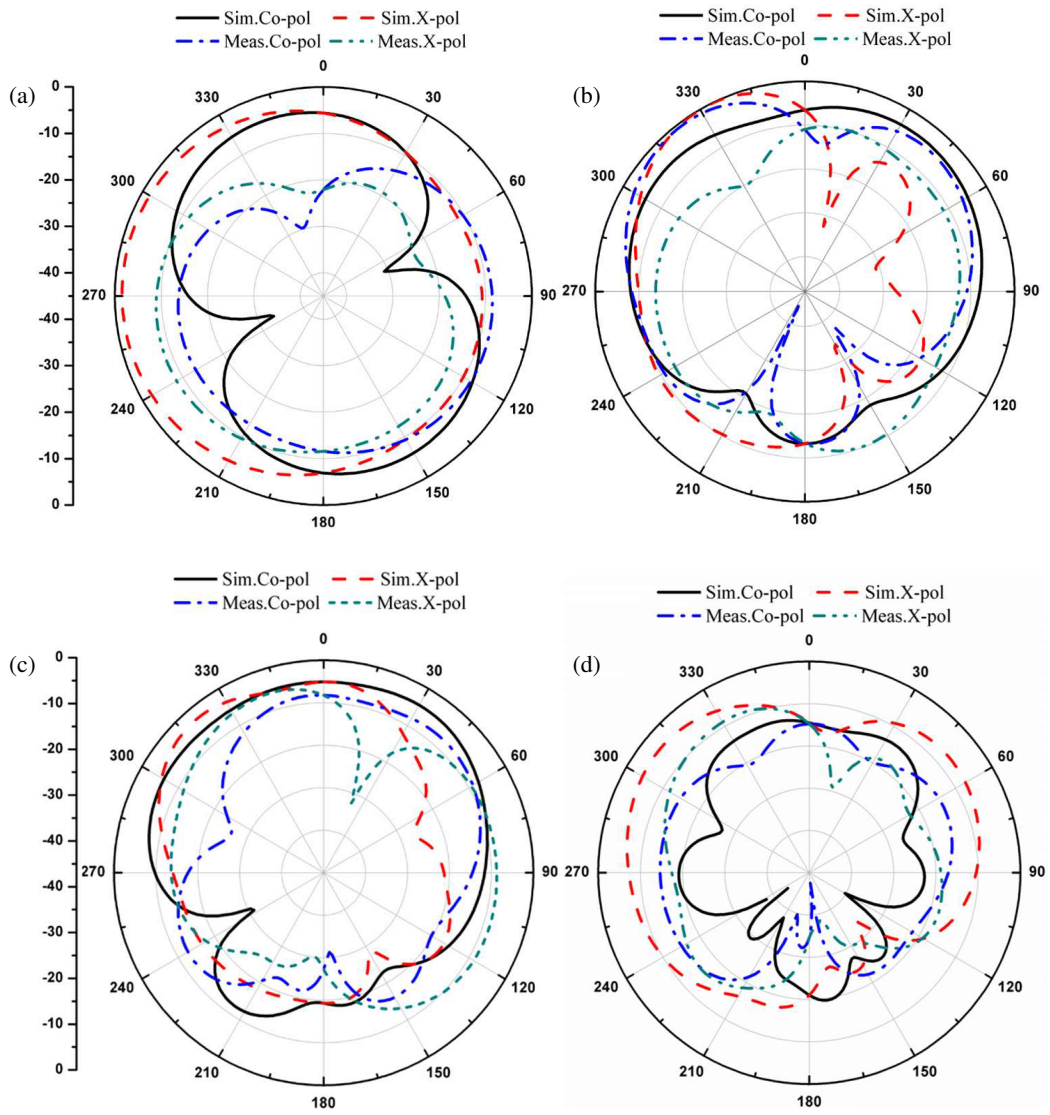

FIGURE 9. Radiating patterns of the proposed antenna. (a) 2.44 GHz, (b) 2.86 GHz, (c) 3.92 GHz, (d) 4.98 GHz.

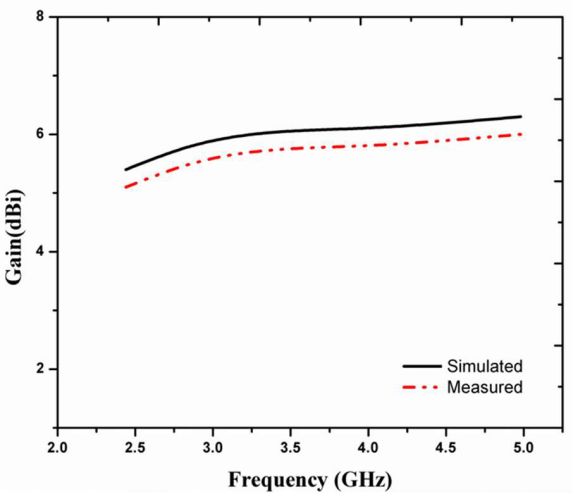

FIGURE 10. Measured gain of the proposed SQCR-DGS design.

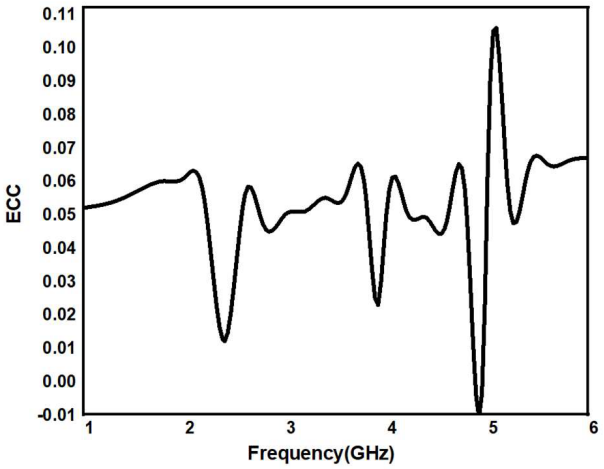

FIGURE 11. ECC of the proposed SQCR-DGS design.

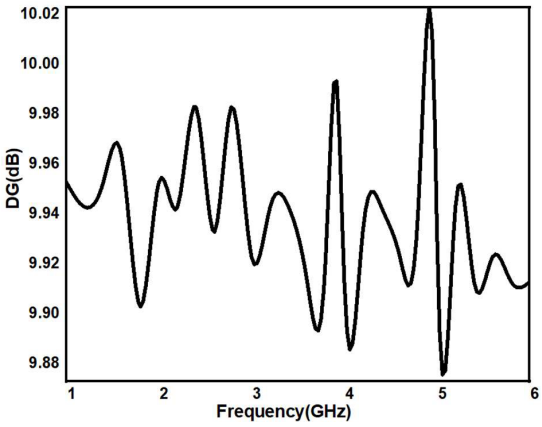

FIGURE 12. DG of the proposed SQCR-DGS design.

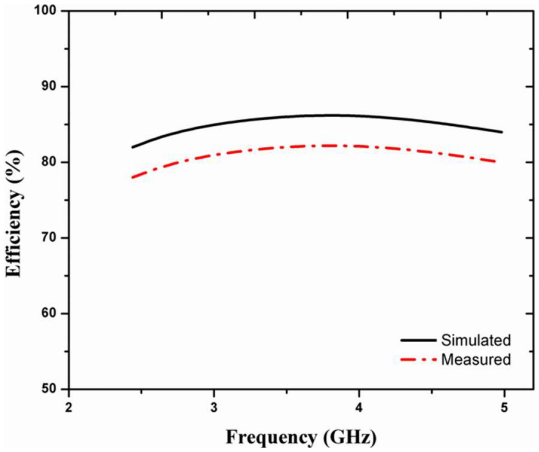

FIGURE 13. Efficiency of the proposed design SQCR-DGS antenna.

TABLE 2. Comparison of SQCR-DGS model with reference to other works.

Ref.	Operating Frequency (GHz)	Reflection Coefficient (dB)	Peak Gain (dB)	Efficiency (%)	ECC	Dimension (mm^3)
[5]	3.56–5.28	−15	2.7	88	0.001	90 × 90 × 1.57
[10]	4.4–5.1	−14	2.8	80	0.04	55 × 55 × 1.6
[13]	4.8–5.0, 5.925–6.4	−17	2.5	82	0.1	158 × 60 × 1.6
[15]	2.23–2.46 3.22–4.04	>−12	3.6 7.1	85	0.025	105 × 105 × 1.83
[23]	4.3–5.0	−16	2.9	84	0.025	65 × 65 × 1.6
[24]	5.925 to 7.125	−38	6	85	NA	50 × 50 × 1.6
[25]	2.32–2.524	−37	4	83	NA	88 × 88
This Work	2.44 GHz 2.86 GHz 3.92 GHz 4.98 GHz	−40.3 −17.9 −14.9 −10.6	5.4 5.8 6.1 6.3	87	0.1	50 × 50 × 1.6

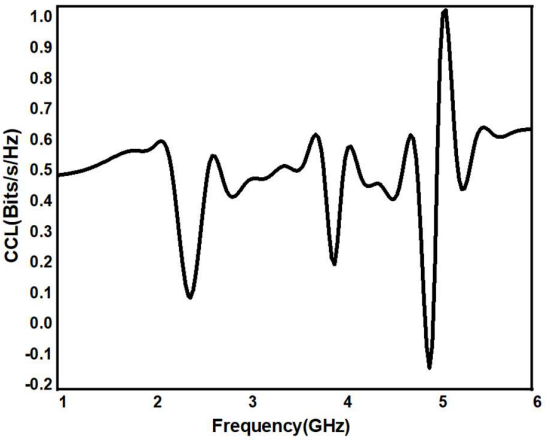

FIGURE 14. CCL of the SQCR-DGS design.

slots, which produce many resonances in a confined space. In addition to this, it keeps the ground currents clear, which means that no additional isolation structures are necessary. Table 2 clearly shows that the proposed antenna provides a good trade-off among compact size, gain, impedance matching, radiation efficiency, and diversity performance compared with previously reported designs. Some reported designs achieve high isolation, but they require larger antenna dimensions or more complicated structures. The proposed antenna can achieve satisfactory performance with a compact and simple design.

4. CONCLUSION

The symmetric arrangement of four circular radiating elements ensures balanced current distribution and stable radiation characteristics, while the semicircular bridge and DGS modify the current paths to produce multiple resonant modes. The proposed antenna provides impedance bandwidths of 2.24–2.94 GHz, 3.84–3.98 GHz, and 4.92–5.06 GHz, with resonant frequencies observed at 2.44 GHz (−40.3 dB), 2.86 GHz (−17.9 dB), 3.92 GHz (−14.9 dB), and 4.98 GHz (−10.6 dB). These operating bands support WLAN, ISM band, and sub-

6 GHz wireless communication systems. The antenna achieves a realized gain exceeding 5 dB across the operating bands and maintains stable radiation efficiency. In addition, diversity performance analysis shows that the envelope correlation coefficient (ECC) remains below 0.5, while the diversity gain varies between 9.88 and 10.02 dB, and the channel capacity loss (CCL) stays below 0.6 bits/s/Hz. These results demonstrate that the proposed antenna offers reliable radiation characteristics and effective diversity performance, making it suitable for practical multi-band wireless communication devices.

REFERENCES

[1] Rekha, S. and G. S. Let, "Design and SAR analysis of wearable UWB MIMO antenna with enhanced isolation using a parasitic structure," *Iranian Journal of Science and Technology, Transactions of Electrical Engineering*, Vol. 46, No. 2, 291–301, 2022.

[2] Yin, W., S. Chen, J. Chang, C. Li, and S. K. Khamas, "CPW fed compact UWB 4-element MIMO antenna with high isolation," *Sensors*, Vol. 21, No. 8, 2688, 2021.

[3] Potti, D., Y. Tusharika, M. G. N. Alsath, S. Kirubaveni, M. Kanagasabai, R. Sankararajan, S. Narendhiran, and P. B. Bhargav, "A novel optically transparent UWB antenna for automotive MIMO communications," *IEEE Transactions on Antennas and Propagation*, Vol. 69, No. 7, 3821–3828, 2021.

[4] Khan, A. A., S. A. Naqvi, M. S. Khan, and B. Ijaz, "Quad port miniaturized MIMO antenna for UWB 11 GHz and 13 GHz frequency bands," *AEU — International Journal of Electronics and Communications*, Vol. 131, 153618, 2021.

[5] Upadhyaya, T., V. Sorathiya, S. Al-Shathri, W. El-Shafai, U. Patel, K. V. Pandya, and A. Armghan, "Quad-port MIMO antenna with high isolation characteristics for sub 6-GHz 5G NR communication," *Scientific Reports*, Vol. 13, No. 1, 19088, 2023.

[6] Khan, I., X. Qi, Y. Shao, K. Zhang, C. Song, M. M. Kamal, and Q. Wu, "Hybrid technique-based circularly polarized MIMO antenna with low mutual coupling for millimeter-wave communications," *Optics Express*, Vol. 33, No. 8, 17 782–17 801, 2025.

[7] Althuwayb, A. A., "Low-interacted multiple antenna systems based on metasurface-inspired isolation approach for MIMO applications," *Arabian Journal for Science and Engineering*, Vol. 47, No. 3, 2629–2638, 2022.

[8] Raza, M. U., K. Zhang, Z. M. Yetneberk, and S. Yan, "Four-port circularly polarized antenna array with enhanced isolation and polarization conversion using metasurface for 5G communications," *Optics Express*, Vol. 32, No. 25, 45 315–45 329, 2024.

[9] Lee, J., H. Kim, and J. Oh, "Large-aperture metamaterial lens antenna for multi-layer MIMO transmission for 6G," *IEEE Access*, Vol. 10, 20 486–20 495, 2022.

[10] Yousef, B. M., A. M. Ameen, A. Desai, H.-T. Hsu, V. Dhasarathan, and A. A. Ibrahim, "Defected ground structure-based wideband circularly polarized 4-port MIMO antenna for future Wi-Fi 6E applications," *AEU — International Journal of Electronics and Communications*, Vol. 170, 154815, 2023.

[11] Tiwari, R. N., R. Thirumalaiah, V. R. Naidu, G. Sreenivasulu, P. Singh, and S. Rajasekaran, "Compact dual band 4-port MIMO antenna for 5G sub-6 GHz/N38/N41/N90 and WLAN frequency bands," *AEU — International Journal of Electronics and Communications*, Vol. 171, 154919, 2023.

[12] Tulum, M. A., A. S. Turk, and P. Mahouti, "Data driven surrogate modeling of phase array antennas using deep learning for millimetric band applications," *IEEE Access*, Vol. 11, 114 415–114 423, 2023.

[13] Zahid, M., Q. Ali, N. Bhowmike, D. P. Bolla, S. Shoaib, and Y. Amin, "Dual-band MIMO antenna for n79 and sub-7 GHz smartphone applications," *Electronics*, Vol. 13, No. 14, 2724, 2024.

[14] Hu, K., Y. Zhou, S. K. Sitaraman, and M. M. Tentzeris, "Additively manufactured flexible on-package phased array antennas for 5G/mmWave wearable and conformal digital twin and massive MIMO applications," *Scientific Reports*, Vol. 13, No. 1, 12515, 2023.

[15] Desai, A., T. Upadhyaya, M. Palandoken, and C. Gocen, "Dual band transparent antenna for wireless MIMO system applications," *Microwave and Optical Technology Letters*, Vol. 61, No. 7, 1845–1856, 2019.

[16] Khan, S., S. N. K. Marwat, M. A. Khan, S. Ahmed, N. Gohar, M. E. Alim, A. D. Algarni, and H. Elmannai, "A self-decoupling technique to realize dense packing of antenna elements in MIMO arrays for wideband sub-6 GHz communication systems," *Sensors*, Vol. 23, No. 2, 654, 2023.

[17] Fang, Y., Y. Jia, J.-Q. Zhu, Y. Liu, and J. An, "Self-decoupling, shared-aperture, eight-antenna MIMO array with MIMO-SAR reduction," *IEEE Transactions on Antennas and Propagation*, Vol. 72, No. 2, 1905–1910, 2024.

[18] Kulkarni, N., R. M. Linus, and N. B. Bahadure, "A small wideband inverted L-shaped flexible antenna for sub-6 GHz 5G applications," *AEU — International Journal of Electronics and Communications*, Vol. 159, 154479, 2023.

[19] Ameen, A. M., M. I. Ahmed, H. Elsadek, and W. R. Anis, "Design of 4-direction MIMO Vivaldi antenna system for vehicles communication in 5G applications," *Journal of Electromagnetic Waves and Applications*, Vol. 36, No. 14, 2027–2040, 2022.

[20] Babu, K. V., P. S. Rao, B. C. Naik, and B. R. Kumar, "Compact dual-band design and analysis of half-circular U-shape MIMO radiator for wireless applications," *Microsystem Technologies*, Vol. 29, No. 4, 501–514, 2023.

[21] Menath, A., V. Kumar, A. Chandra, and R. Kumar, "Multi band miniaturized 2×2 MIMO antenna for sub-6-GHz applications," *IEEE Access*, Vol. 14, 13 948–13 956, 2026.

[22] Hemalatha, T. and B. Roy, "Low-profile CO-CSRR and EBG loaded tri-quarter circular patch EWB MIMO antenna with multiple notch bands," *IEEE Open Journal of Antennas and Propagation*, Vol. 5, No. 3, 634–643, 2024.

[23] Das, G. S., B. B. Chamuah, Y. Beria, P. P. Kalita, and A. Buragohain, "Compact four elements sub-6 GHz MIMO antenna for 5G applications," *Materials Today: Proceedings*, 2023.

[24] Ramal, P. J., S. N. S. Althaf, K. Vishnulakshmi, P. Sundaravadivel, and R. Dhandapani, "A compact wide-band circular slot quad-port MIMO antenna for 5G wireless applications," *Progress In Electromagnetics Research Letters*, Vol. 120, 65–71, 2024.

[25] Kolte, J. C., A. Kumar, and P. Bansal, "Designing MIMO antenna with high isolation decoupling structure," *Progress In Electromagnetics Research B*, Vol. 113, 37–50, 2025.